Theory Probab. Appl.
Vol. 64, No. 4, pp. xx–xx

WEIGHTED POISSON–DELAUNAY MOSAICS*

H. EDELSBRUNNER† AND A. NIKITENKO†

Abstract. Slicing a Voronoi tessellation in $\mathbf{R}^n$ with a k-plane gives a k-dimensional weighted Voronoi tessellation, also known as a power diagram or Laguerre tessellation. Mapping every simplex of the dual weighted Delaunay mosaic to the radius of the smallest empty circumscribed sphere whose center lies in the k-plane gives a generalized discrete Morse function. Assuming the Voronoi tessellation is generated by a Poisson point process in $\mathbf{R}^n$, we study the expected number of simplices in the k-dimensional weighted Delaunay mosaic as well as the expected number of intervals of the Morse function, both as functions of a radius threshold. As a by-product, we obtain a new proof for the expected number of connected components (*clumps*) in a line section of a circular Boolean model in $\mathbf{R}^n$.

Key words. Voronoi tessellations, Laguerre distance, weighted Delaunay mosaics, discrete Morse theory, critical simplices, intervals, stochastic geometry, Poisson point process, Boolean model, clumps, Slivnyak–Mecke formula, Blaschke–Petkantschin formula

DOI. 10.1137/S0040585X97T989726

1. Introduction. Given a discrete set of points $Y \subseteq \mathbf{R}^k$, the *Voronoi tessellation* tiles the k-dimensional Euclidean space with convex polyhedra, each consisting of all points $a \in \mathbf{R}^k$ for which a particular point y is the closest among all points in Y. To generalize, suppose each $y \in Y$ has a weight $w_y \in \mathbf{R}$, and substitute the *power distance* of a from y, defined as $\|a-y\|^2 - w_y$, for the squared Euclidean distance in the definition of the Voronoi tessellation. The resulting tiling of $\mathbf{R}^k$ into convex polyhedra is known under several names, including *power diagrams* [1] and *Laguerre tessellations* [13], but to streamline language we call them *weighted Voronoi tessellations*. They do indeed look like unweighted Voronoi tessellations, except that the hyperplane separating two neighboring polyhedra does not necessarily lie halfway between the generating points; see Figure 1. Our motivation for studying weighted Voronoi tessellations derives from the extra degree of freedom — the weight — which permits better approximations of observed tilings, such as cell cultures in plants [19] and microstructures of materials [4]. Beyond this practical consideration, there is an intriguing connection between the volumes of skeleta of unweighted Voronoi tessellations and the number of simplices in weighted Delaunay mosaics through the Crofton formula, which is worth exploring. We discuss it at the end of section 5.

Our preferred construction takes a k-dimensional slice through a Voronoi tessellation in $\mathbf{R}^n$ (see [2], [21]). Specifically, if X is a discrete set of points in $\mathbf{R}^n$, and $\mathbf{R}^k \hookrightarrow \mathbf{R}^n$ is spanned by the first $k \leqslant n$ coordinate axes, then the Voronoi tessellation of X in $\mathbf{R}^n$ intersects $\mathbf{R}^k$ in a k-dimensional weighted Voronoi tessellation. The points in $\mathbf{R}^k$ that generate the weighted tessellation are the orthogonal projections y_x of the points $x \in X$, and their weights are $w_x = -\|x - y_x\|^2$. While all the weights in this construction are nonpositive, this is not a restriction of generality because

*Received by the editors March 17, 2016. This project was supported by the European Research Council (ERC) under the European Union's Horizon 2020 research and innovation programme (grant agreement 78818 Alpha), and was partially supported by the DFG Collaborative Research Center TRR 109, "Discretization in Geometry and Dynamics" and by grant I02979-N35 of the Austrian Science Fund (FWF). Originally published in the Russian journal *Teoriya Veroyatnostei i ee Primeneniya*, 64 (2019), pp. 746–770.

https://doi.org/10.1137/S0040585X97T989726

†Institute of Science and Technology Austria, Klosterneuburg, Austria (edels@ist.ac.at, anton.nikitenko@ist.ac.at).

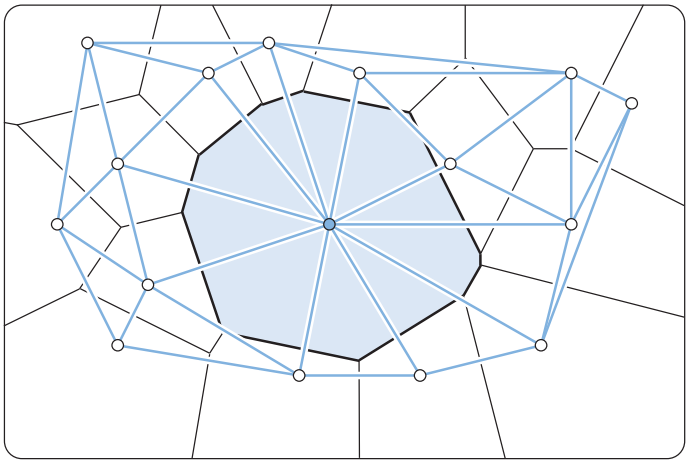

FIG. 1. *Weighted Voronoi tessellation in* $\mathbf{R}^2$ *with superimposed weighted Delaunay mosaic. All points have zero weight except the point with the shaded domain, which has positive weight.*

the tessellation remains unchanged when all the weights are increased by the same amount. Indeed, every weighted Voronoi tessellation with bounded weights can be obtained as a slice of an unweighted Voronoi tessellation. It is often more convenient to consider the dual of a weighted Voronoi tessellation, which is again known under several names, including *Laguerre triangulation* [17] and *regular triangulation* [9], but we call them *weighted Delaunay mosaics*. An important difference to the unweighted concept is that the Voronoi polyhedron of a weighted point may be empty, in which case this weighted point is not a vertex of the weighted Delaunay mosaic. For generic sets of weighted points, the weighted Delaunay mosaic is a simplicial complex in $\mathbf{R}^k$. Since we focus on slices of unweighted Voronoi tessellations, we define the general position only in this case. Specifically, we say that a discrete set $X \subseteq \mathbf{R}^n$ is *generic* if the following conditions are satisfied for every $0 \leqslant j < n$:

(a) no $j+2$ points belong to a common j-plane;

(b) no $j+3$ points belong to a common j-sphere;

(c) considering a unique j-sphere that passes through $j+2$ points, no $j+1$ of these points belong to a j-plane that passes through the center of the j-sphere;

(d) considering a unique j-plane that passes through $j+1$ points, this plane is neither orthogonal nor parallel to $\mathbf{R}^k$;

(e) no two points have identical distance to $\mathbf{R}^k$.

For $j = 0$, property (d) means that no point of X is in $\mathbf{R}^k$. We note that the Poisson point process is generic with probability 1.

Continuing the work started in [7], we are interested in the stochastic properties of the weighted Delaunay mosaics and their radius functions. To explain the latter concept, we assume the generic case in which the mosaic is a simplicial complex, and for every simplex $Q' \in \operatorname{Del} Y$ with preimage $Q \subseteq \mathbf{R}^n$, we find the smallest $(n-1)$-sphere that satisfies the following properties:

(i) It passes through all vertices of Q (it is a *circumscribed sphere* of Q),

(ii) the open ball it bounds does not contain any points of X (it is *empty*), and

(iii) its center lies in $\mathbf{R}^k$ (it is *anchored*).

The existence of such spheres for the simplices of the weighted mosaic can be shown in a way similar to the unweighted case [5] and is left to the reader. We

call this sphere the *weighted Delaunay sphere*, and its radius the *weighted Delaunay radius* of $Q' \in \operatorname{Del} Y$. Similarly, when considering Q instead of Q', we call this sphere the *anchored Delaunay sphere*, and its center the *anchor* of Q. The *radius function* of the weighted Delaunay mosaic, $\mathcal{R}\colon \operatorname{Del} Y \to \mathbf{R}$, maps every simplex to its weighted Delaunay radius. As in the unweighted case, it partitions $\operatorname{Del} Y$ into *intervals* of simplices that share the same weighted Delaunay sphere and, therefore, the same function value [3]. These intervals have topological significance [8]: adding the simplices in the order of increasing radius, the homotopy type of the complex changes whenever the interval contains a single simplex, and it remains unchanged whenever the interval contains two or more simplices. Indeed, the operation in the latter case is known as *anticollapse* and has been studied extensively in combinatorial topology. Each interval is defined by two simplices $L \subseteq U$ in the weighted Delaunay mosaic and consists of all simplices that contain L and are contained in U. We call $Q' \in \operatorname{Del} Y$ a *critical simplex* of $\mathcal{R}$ if it is the sole simplex in its interval, $L = Q' = U$, and we call Q' a *regular simplex* of $\mathcal{R}$ otherwise. The *type* of the interval is the pair of dimensions of the lower and the upper bounds, (ℓ, m), in which $\ell = \dim L$ and $m = \dim U$. Our main result is an extension of the stochastic findings about the radius function of the Poisson–Delaunay mosaic in [7] from the unweighted to the weighted case.

THEOREM 1 (main result). *Let X be a Poisson point process with density ρ in $\mathbf{R}^n$ and $\mathbf{R}^k \hookrightarrow \mathbf{R}^n$. There are constants $C_{\ell,m}^{k,n}$ such that, for any $r_0 \geqslant 0$, the expected number of intervals of type (ℓ, m) in the k-dimensional weighted Poisson–Delaunay mosaic with center in a Borel set $\Omega \subseteq \mathbf{R}^k$ and weighted Delaunay radius at most r_0 is*

$$\mathbf{E}[c_{\ell,m}^{k,n}(r_0)] = C_{\ell,m}^{k,n} \frac{\gamma(m+1-k/n;\, \rho\nu_n r_0^n)}{\Gamma(m+1-k/n)} \rho^{k/n} \|\Omega\|, \tag{1}$$

in which ν_n is the volume of the unit ball in $\mathbf{R}^n$, and we give explicit computations of the constants in $k \leqslant 2$ dimensions. Similarly, the expected number of j-dimensional simplices in the weighted Poisson–Delaunay mosaic with center in a Borel set $\Omega \subseteq \mathbf{R}^k$ and weighted Delaunay radius at most r_0 is

$$\mathbf{E}[d_j^{k,n}(r_0)] = \left[\sum_{m=j}^{k} \frac{\gamma(m+1-k/n;\, \rho\nu_n r_0^n)}{\Gamma(m+1-k/n)} \sum_{\ell=0}^{j} \binom{m-\ell}{m-j} C_{\ell,m}^{k,n} \right] \rho^{k/n} \|\Omega\|. \tag{2}$$

Some of the values for constants $C_{\ell,m}^{k,n}$ are listed in Tables 1 and 2 (see sections 2 and 6, respectively). In an equivalent formulation, this theorem states that the weighted Delaunay radius of a *typical interval* is Gamma-distributed, whereas the weighted Delaunay radius of a *typical simplex* is a mixture of Gamma distributions; cf. [7]. In a more general context, the contributions of this paper apply to the field of stochastic geometry; see the book by Schneider and Weil [20] for a basic review of this field. The particular questions on Poisson–Delaunay mosaics studied in this paper were pioneered by Miles almost 50 years ago (see [14], [15]). Formulas for the weighted case have also been derived by Møller [16], but these are restricted to top-dimensional simplices whose expected numbers can be derived using the Crofton formula and expected volumes of Voronoi skeleta.

Outline. Section 2 discusses the case $k = 1$ as a warm-up exercise. It is sufficiently elementary so that explicit formulas can be derived without reliance on more difficult ones to prove general integral formulas. Section 3 shows how to get

the expected number of connected components in the intersection of a line with a circular Boolean model in $\mathbf{R}^n$ using the discrete Morse theory. Section 4 proves a Blaschke–Petkantschin type formula for the general weighted case. Section 5 uses this formula to prove our main result. Section 6 develops explicit expressions for all types of intervals in two dimensions. Section 7 concludes this paper. Appendix A introduces the special functions and distributions used in the derivation of our results.

2. One dimension. In $k = 1$ dimension, the weighted Delaunay mosaic has a simple structure, and so results can be obtained by elementary means.

Slice construction. Let $n \geqslant 2$, and let $X \subseteq \mathbf{R}^n$ be a stationary Poisson point process with density $\rho > 0$. We write $\mathbf{R}^1 \hookrightarrow \mathbf{R}^n$ for the first coordinate axis, which is a directed line passing through $\mathbf{R}^n$. For each point $x = (x_1, x_2, \ldots, x_n) \in X$, we write $y_x = (x_1, 0, \ldots, 0)$ for the projection onto $\mathbf{R}^1$, and $-w_x = x_2^2 + x_3^2 + \cdots + x_n^2$ for its squared distance from the line. Denoting by $Y = \{(y_x, w_x) \mid x \in X\}$ the resulting set of weighted points in $\mathbf{R}^1$, we are interested in its weighted Voronoi tessellation, $\operatorname{Vor} Y$, and its weighted Delaunay mosaic, $\operatorname{Del} Y$. By construction, the former is the intersection of the n-dimensional (unweighted) Voronoi tessellation with the line: $\operatorname{Vor} Y = \{\operatorname{domain}(x) \cap \mathbf{R}^1 \mid x \in X\}$. As discussed above, the interval $\operatorname{domain}(x) \cap \mathbf{R}^1$ belongs to the weighted Voronoi tessellation if and only if there is an anchored Delaunay sphere of x, that is, an empty sphere centered in $\mathbf{R}^1$ that passes through x. Similarly, two weighted Voronoi domains, $\operatorname{domain}(x) \cap \mathbf{R}^1$ and $\operatorname{domain}(u) \cap \mathbf{R}^1$, share an endpoint if and only if there is an empty anchored Delaunay sphere passing through x and u. It follows that every edge in $\operatorname{Del} Y$ is the projection of an edge in $\operatorname{Del} X$; see Figure 2.

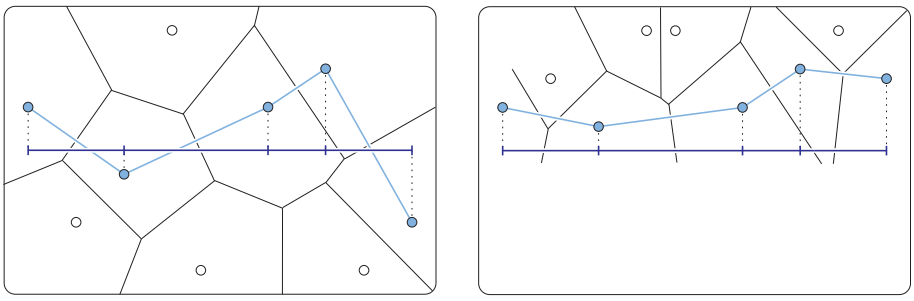

FIG. 2. *Left*: *a* 1*-dimensional weighted Voronoi tessellation as a slice of a* 2*-dimensional unweighted Voronoi tessellation. The weighted Delaunay mosaic in* $\mathbf{R}^1$ *is the projection of a chain of edges in the* 2*-dimensional unweighted Delaunay mosaic. Right*: *reflecting the points across* $\mathbf{R}^1$ *affects the* 2*-dimensional Voronoi tessellation but not the* 1*-dimensional slice.*

As suggested in Figure 2, we can simplify the construction by reducing n to 2. Writing $\mathbf{H}$ for the half-plane of points, whose first coordinate is arbitrary, whose second coordinate is nonnegative, and whose remaining $n - 2$ coordinates vanish, we map $x = (x_1, \ldots, x_n) \in \mathbf{R}^n$ to $x' = (x_1, \sum_{i=2}^n x_i^2, 0, \ldots, 0) \in \mathbf{H}$. This amounts to rotating x around $\mathbf{R}^1$ into $\mathbf{H}$. Let X' be the resulting set of points in $\mathbf{H}$, and let Y' be the set of weighted points in $\mathbf{R}^1$ obtained by projection from X'. Then $Y = Y'$, which shows that X and X' define the same 1-dimensional weighted Voronoi tessellation and weighted Delaunay mosaic. There is a small price to pay for the simplification, namely that the projected Poisson point process in $\mathbf{H}$ is not necessarily homogeneous. Specifically, the projected process in $\mathbf{H}$ is a Poisson point process with

intensity $\varrho(x) = \sigma_{n-1}\rho x_2^{n-2}$, in which σ_{n-1} is the $(n-2)$-dimensional volume of the unit sphere in $\mathbf{R}^{n-1}$.

Interval structure. We now return to the intervals of the radius function in one dimension, $\mathcal{R}\colon \operatorname{Del} Y \to \mathbf{R}$. In the assumed generic case, $\operatorname{Del} Y$ contains only two kinds of simplices: vertices and edges. By definition, the value of $\mathcal{R}$ at a simplex $Q' \in \operatorname{Del} Y$ is the radius of the anchored Delaunay sphere of the preimage of Q'. There are only three types of intervals $[L, U]$ as follows:

$(0, 0)$: Here $L = U$ and $\dim L = \dim U = 0$. The interval contains a single and, therefore, critical vertex.

$(1, 1)$: Here $L = U$ and $\dim L = \dim U = 1$. The interval contains a single and, therefore, critical edge.

$(0, 1)$: Here $L \subseteq U$ and $\dim L = \dim U - 1$. The interval is a pair consisting of a regular vertex and a regular edge. We call it a *vertex-edge pair* if the vertex precedes the edge as we go from left to right, and we call it an *edge-vertex pair* otherwise.

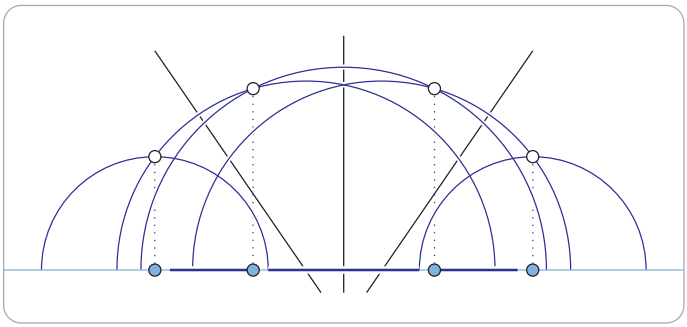

FIG. 3. *From left to right on the horizontal line*: *a critical vertex*, *an edge-vertex pair*, *a critical edge*, *a vertex-edge pair*, *and another critical vertex.*

The cases can be distinguished geometrically, as illustrated in Figure 3. Let $x = (x_1, x_2) \in \mathbf{H}$ and $y_x = (x_1, 0)$ with weight $w_x = -x_2^2$. Then $L = U = \{y_x\}$ is a critical vertex of $\operatorname{Del} Y$ if and only if y_x is the anchor of x. Otherwise, the anchored Delaunay circle of x also passes through a second point, $u \in X \subseteq \mathbf{H}$, with y_x and y_u on the same side of the anchor. In this case, $L = \{y_x\}$ and $U = \{y_x, y_u\}$ form a vertex-edge or an edge-vertex pair. Finally, we have a critical edge $L = U = \{y_x, y_u\}$ if y_x and y_u lie on opposite sides of the anchor.

We make essential use of the geometric characterization of interval types when we compute their expected numbers. To simplify the computation, we note that the structure along $\mathbf{R}^1$ is a strict repetition of the following pattern: a critical vertex, a nonnegative number of edge-vertex pairs, a critical edge, and a nonnegative number of vertex-edge pairs.

Critical vertices. We begin with computing the number of critical vertices, $c_{0,0}^{1,n}$, inside a region $\Omega \subseteq \mathbf{R}^1$ and with weighted Delaunay radius at most some threshold r_0. Let $x = (x_1, x_2) \in X \subseteq \mathbf{H}$, and note that the smallest anchored circle passing through x has the center $y_x = (x_1, 0)$ and the radius $r = x_2$. Write $\mathbf{P}_\varnothing(x)$ for the probability that this circle is empty, $\mathbf{1}_\Omega(x)$ for the indicator that $y_x \in \Omega$, and $\mathbf{1}_{r_0}(x)$ for the indicator that $r \leqslant r_0$. We use the Slivnyak–Mecke formula to compute

$$\mathbf{E}[c_{0,0}^{1,n}(r_0)] = \int_{x \in \mathbf{H}} \mathbf{1}_\Omega(x)\mathbf{1}_{r_0}(x)\mathbf{P}_\varnothing(x)\varrho(x)\,\mathrm{d}x; \tag{3}$$

cf. [7]. The intensity measure of the upper semicircle with radius r is of course ρ times the volume of an n-ball with radius r, which we write as $\rho\nu_r r^n$. Hence $\mathbf{P}_\varnothing(x) = e^{-\rho\nu_n r^n}$. In other words, the probability that the anchored circle is empty is the probability that the n-ball, whose points get rotated into the semidisk, is empty. So we have

$$\begin{aligned}\mathbf{E}[c^{1,n}_{0,0}(r_0)] &= \int_{x_1\in\Omega}\int_{r=0}^{r_0} e^{-\rho\nu_n r^n}\rho\sigma_{n-1}r^{n-2}\,\mathrm{d}r\,\mathrm{d}x_1\\ &= \|\Omega\|\sigma_{n-1}\rho\int_{r=0}^{r_0} r^{n-2}e^{-\rho\nu_n r^n}\,\mathrm{d}r. \qquad (4)\end{aligned}$$

To evaluate this integral, we use the identity on Gamma functions proved in Lemma 2 in Appendix A, where the functions are defined. In this application, the integral on the right of (4) evaluates to $\gamma(1-1/n;\,\rho\nu_n r_0^n)/[n\cdot(\rho\nu_n)^{1-1/n}]$. Writing $c^{1,n}_{0,0} = c^{1,n}_{0,0}(\infty)$, we set $r_0 = \infty$ to get the expected total number of critical vertices, and we write the expected number up to weighted Delaunay radius r_0 as a fraction of the former:

$$\mathbf{E}[c^{1,n}_{0,0}] = \frac{\sigma_{n-1}\Gamma(1-1/n)}{n\nu_n^{1-1/n}}\|\Omega\|\rho^{1/n}, \qquad (5)$$

$$\mathbf{E}[c^{1,n}_{0,0}(r_0)] = \frac{\gamma(1-1/n;\,\rho\nu_n r_0^n)}{\Gamma(1-1/n)}\mathbf{E}[c^{1,n}_{0,0}]. \qquad (6)$$

Regular edges. To count the regular edges (or intervals of type $(0,1)$) we again use the Slivnyak–Mecke formula. Let $x = (x_1, x_2)$ and $u = (u_1, u_2)$ be two points in $X \subseteq \mathbf{H}$. There is a unique anchored circle that passes through both points, and the edge connecting y_x and y_u belongs to $\operatorname{Del} Y$ if and only if this circle is empty. Writing $(z_1, 0)$ for the center and r for the radius, the edge is critical if $x_1 < z_1 < u_1$; otherwise it is regular; see Figure 3. Write $\mathbf{P}_\varnothing(x,u)$ for the probability that a unique anchored circle passing through x and u is empty, $\mathbf{1}_\Omega(x,u)$ for the indicator that $z_1 \in \Omega$, $\mathbf{1}_{r_0}(x,u)$ for the indicator that $r \leqslant r_0$, and $\mathbf{1}_{0,1}(x,u)$ for the indicator that x_1 and u_1 lie on the same side of z_1. By the Slivnyak–Mecke formula,

$$\mathbf{E}[c^{1,n}_{0,1}(r_0)] = \frac{1}{2!}\int_{u\in\mathbf{H}}\int_{x\in\mathbf{H}} \mathbf{1}_\Omega(x,u)\mathbf{1}_{r_0}(x,u)\mathbf{1}_{0,1}(x,u)\mathbf{P}_\varnothing(x,u)\varrho(x)\varrho(u)\,\mathrm{d}x\,\mathrm{d}u. \qquad (7)$$

We already know that $\mathbf{P}_\varnothing(x,u) = e^{-\rho\nu_n r^n}$. To compute the rest, we do a change of variables, reparametrizing the points by the center and radius of a unique anchored circle passing through them and two angles, $x = (z_1 + r\cos\xi,\, r\sin\xi)$ and $u = (z_1 + r\cos\upsilon,\, r\sin\upsilon)$, in which $0 \leqslant \xi, \upsilon < \pi$. This is a bijection up to a set of measure 0. The Jacobian of this change of variables is the absolute determinant of the matrix of old variables derived by the new variables:

$$J = \operatorname{abs}\begin{bmatrix} 1 & \cos\xi & -r\sin\xi & 0\\ 0 & \sin\xi & r\cos\xi & 0\\ 1 & \cos\upsilon & 0 & -r\sin\upsilon\\ 0 & \sin\upsilon & 0 & r\cos\upsilon\end{bmatrix} = r^2|\cos\upsilon - \cos\xi|. \qquad (8)$$

With the new variables, the indicators can be absorbed into integration limits as follows: $\mathbf{1}_\Omega(x,u) = 1$ if and only if $z_1 \in \Omega$, and $\mathbf{1}_{0,1}(x,u) = 1$ if and only if ξ and υ are either both smaller or both larger than $\pi/2$. The two cases are symmetric, so we

assume the former and multiply by 2. The integral in (7) thus turns into

$$\begin{aligned}\mathbf{E}[c_{0,1}^{1,n}(r_0)] &= \int_{z_1\in\Omega}\int_{r=0}^{r_0} e^{-\rho\nu_n r^n}\int_{0\leqslant\xi,\,\upsilon<\pi/2}\rho^2\sigma_{n-1}^2(r^2\sin\xi\sin\upsilon)^{n-2}r^2 \\ &\quad\times|\cos\upsilon-\cos\xi|\,\mathrm{d}\xi\,\mathrm{d}\upsilon\,\mathrm{d}r\,\mathrm{d}z_1 \qquad (9)\\ &= \|\Omega\|\rho^2\sigma_{n-1}^2\int_{r=0}^{r_0} e^{-\rho\nu_n r^n}r^{2n-2}\,\mathrm{d}r\int_{0\leqslant\xi,\,\upsilon<\pi/2}(\sin\xi\sin\upsilon)^{n-2} \\ &\quad\times|\cos\upsilon-\cos\xi|\,\mathrm{d}\xi\,\mathrm{d}\upsilon. \qquad (10)\end{aligned}$$

We apply Lemma 2 to evaluate the integral over the radius, and we use Mathematica software to evaluate the integral over the two angles:

$$\int_{r\leqslant r_0} r^{2n-2}e^{-\rho\nu_n r^n}\,\mathrm{d}r = \frac{\gamma(2-1/n;\,\rho\nu_n r_0^n)}{n(\rho\nu_n)^{2-1/n}}, \qquad (11)$$

$$\begin{aligned}&\int_{0\leqslant\xi,\,\upsilon<\pi/2}(\sin\xi\sin\upsilon)^{n-2}|\cos\upsilon-\cos\xi|\,\mathrm{d}\xi\,\mathrm{d}\upsilon \\ &\qquad= \frac{\sqrt{\pi}}{n-1}\left[\frac{2\Gamma(n-1)}{\Gamma(n-1/2)}-\frac{\Gamma((n-1)/2)}{\Gamma(n/2)}\right]. \qquad (12)\end{aligned}$$

Setting $r_0=\infty$, we get the expected total number of regular edges, and as before we write the expected number up to weighted Delaunay radius r_0 as a fraction of the total number:

$$\mathbf{E}[c_{0,1}^{1,n}] = \frac{\sigma_{n-1}^2\Gamma(2-1/n)}{n\nu_n^{2-1/n}}\,\frac{\sqrt{\pi}}{n-1}\left[\frac{2\Gamma(n-1)}{\Gamma(n-1/2)}-\frac{\Gamma((n-1)/2)}{\Gamma(n/2)}\right]\|\Omega\|\rho^{1/n}, \qquad (13)$$

$$\mathbf{E}[c_{0,1}^{1,n}(r_0)] = \frac{\gamma(2-1/n;\,\rho\nu_n r_0^n)}{\Gamma(2-1/n)}\mathbf{E}[c_{0,1}^{1,n}]. \qquad (14)$$

Summary. Recall that the critical vertices and the critical edges alternate along $\mathbf{R}^1$, which implies that their expected total number is the same. The dependence on the radius threshold, r_0, however, is different. Here we notice that the dependence on the radius for $c_{1,1}^{1,n}$ is the same as for $c_{0,1}^{1,n}$ because only the admissible angles change in the integral. Extracting the constants from the formulas for the expectation, we use (5) and (13) to get

$$C_{0,0}^{1,n} = C_{1,1}^{1,n} = \frac{\sigma_{n-1}\Gamma(1-1/n)}{n\nu_n^{1-1/n}}, \qquad (15)$$

$$C_{0,1}^{1,n} = \frac{\sigma_{n-1}^2\sqrt{\pi}\,\Gamma(2-1/n)}{n(n-1)\nu_n^{2-1/n}}\left[\frac{2\Gamma(n-1)}{\Gamma(n-1/2)}-\frac{\Gamma((n-1)/2)}{\Gamma(n/2)}\right]; \qquad (16)$$

see Table 1. We write the expectations as fractions of these constants times the size of the region times the nth root of the density in $\mathbf{R}^n$:

$$\mathbf{E}[c_{0,0}^{1,n}(r_0)] = C_{0,0}^{1,n}\frac{\gamma(1-1/n;\,\rho\nu_n r_0^n)}{\Gamma(1-1/n)}\|\Omega\|\rho^{1/n}, \qquad (17)$$

$$\mathbf{E}[c_{0,1}^{1,n}(r_0)] = C_{0,1}^{1,n}\frac{\gamma(2-1/n;\,\rho\nu_n r_0^n)}{\Gamma(2-1/n)}\|\Omega\|\rho^{1/n}, \qquad (18)$$

$$\mathbf{E}[c_{1,1}^{1,n}(r_0)] = C_{1,1}^{1,n}\frac{\gamma(2-1/n;\,\rho\nu_n r_0^n)}{\Gamma(2-1/n)}\|\Omega\|\rho^{1/n}. \qquad (19)$$

To get the corresponding results for the simplices in the weighted Delaunay mosaic, we note that the number of vertices is $d_0^{1,n} = c_{0,0}^{1,n} + c_{0,1}^{1,n}$ and the number of edges is $d_1^{1,n} = c_{0,1}^{1,n} + c_{1,1}^{1,n}$. The two are the same, but this is not true if we limit the radius to a finite threshold. Indeed, the radius of a typical edge is Gamma-distributed, while the radius of a typical vertex follows a linear combination of two Gamma distributions. In the limit, as $n \to \infty$, the constants are $\lim_{n\to\infty} C_{0,0}^{1,n} = \sqrt{e}$, $\lim_{n\to\infty} C_{0,1}^{1,n} = \sqrt{e}(\sqrt{2}-1)$, and $\lim_{n\to\infty} D_0^{1,n} = \lim_{n\to\infty} D_1^{1,n} = \sqrt{2e}$, which can again be verified using Mathematica.

TABLE 1

The rounded constants in the expressions of the expected number of intervals and simplices of a 1-dimensional weighted Delaunay mosaic. The ratio of the expected number of critical edges over the expected number of regular edges is monotonically decreasing. It follows that we can infer the ambient dimension from the ratio.

	$n=2$	3	4	5	6	7	8	9	...	20	...	∞
$C_{0,0}^{1,n}$	1.00	1.09	1.16	1.22	1.26	1.29	1.32	1.35	...	1.47	...	1.65
$C_{0,1}^{1,n}$	0.27	0.36	0.42	0.45	0.48	0.50	0.51	0.53	...	0.60	...	0.68
$D_0^{1,n}$	1.27	1.46	1.58	1.67	1.74	1.79	1.84	1.87	...	2.07	...	2.33

3. Connection to Boolean model. Let X be a Poisson point process with density ρ in $\mathbf{R}^n$, and write X_r for the union of closed balls of fixed radius r, whose centers are in X. This random set is sometimes referred to as the *Boolean model* [20]. Let $\Omega \subseteq \mathbf{R}^1 \subseteq \mathbf{R}^n$ be a line segment, and consider $X_r \cap \Omega$. We are interested in the connected components in this intersection and claim that their number satisfies $\beta_0(\mathrm{Del}_r(Y;\Omega)) \leqslant \beta_0(X_r \cap \Omega) \leqslant \beta_0(\mathrm{Del}_r(Y;\Omega)) + 2$, in which $\mathrm{Del}_r(Y;\Omega)$ is the subcomplex of the weighted Delaunay mosaic that consists of all simplices with radius at most r, whose weighted Delaunay center lies in Ω. This follows from the general observation that the weighted Delaunay mosaic of a set of points $y \in \mathbf{R}^k$ with weights w_y is homotopy equivalent to the union of power balls, $Y_r = \{a \in \mathbf{R}^k \mid \|a-y\|^2 - w_y \leqslant r^2\}$, and $Y_r \cap \Omega = X_r \cap \Omega$. Indeed, the weighted Delaunay complex can be defined as the nerve of the decomposition of Y_r with the weighted Voronoi tessellation, so the Nerve Theorem asserts the homotopy equivalence; see [6] for details. By restricting the Delaunay mosaic to a line segment, we can lose up to two connected components at the ends of Ω; see Figure 4.

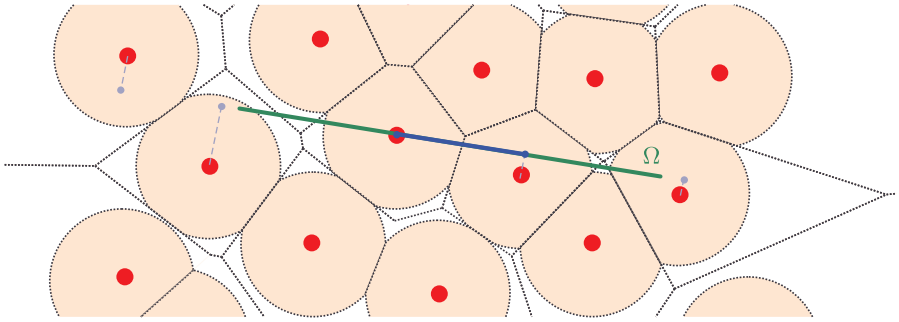

FIG. 4. *Intersection of a union of 2-dimensional balls with a line segment Ω. This intersection has three components, two more than the restricted weighted Delaunay mosaic, which consists of two vertices and the connecting edge in the middle of Ω. The restricted mosaic misses the two tail components because the centers of the corresponding balls do not project into Ω.*

Following the evolution of the nested complexes $\mathrm{Del}_r(Y;\Omega)$, as r goes from 0 to ∞, we observe that upon entering the complex a critical vertex creates a new component, a regular interval does not affect the homotopy type, and a critical edge connects two components; cf. Figure 3. It follows that the expected number of components in $\mathrm{Del}_r(Y;\Omega)$ is

$$\begin{aligned}
&\mathbf{E}[c^{1,n}_{0,0}(r) - c^{1,n}_{1,1}(r)]\\
&\quad= \frac{\sigma_{n-1}\Gamma(1-1/n)}{n\nu_n^{1-1/n}}\left[\frac{\gamma(1-1/n;\,\rho\nu_n r^n)}{\Gamma(1-1/n)} - \frac{\gamma(2-1/n;\,\rho\nu_n r^n)}{\Gamma(2-1/n)}\right]\rho^{1/n}\|\Omega\| \qquad (20)\\
&\quad= \frac{\sigma_{n-1}}{n\nu_n^{1-1/n}}\left[\gamma\left(1-\frac{1}{n};\,\rho\nu_n r^n\right) - \frac{\gamma(2-1/n;\,\rho\nu_n r^n)}{1-1/n}\right]\rho^{1/n}\|\Omega\|. \qquad (21)
\end{aligned}$$

We write $A = \rho\nu_n r^n$, use the definition of the incomplete Gamma function, and integrate by parts to get

$$\begin{aligned}
\gamma(2-1/n;\,A) &= \int_0^A x^{1-1/n}e^{-x}\,\mathrm{d}x\\
&= [-x^{1-1/n}e^{-x}]_0^A + \left(1-\frac{1}{n}\right)\int_0^A x^{-1/n}e^{-x}\,\mathrm{d}x \qquad (22)\\
&= -A^{1-1/n}e^{-A} + \left(1-\frac{1}{n}\right)\gamma\left(1-\frac{1}{n};\,A\right). \qquad (23)
\end{aligned}$$

Noticing that $A^{1-1/n}\rho^{1/n} = (\rho\nu_n r^n)^{1-1/n}\rho^{1/n} = \rho\nu_n^{1-1/n}r^{n-1}$, we plug (23) into (21) to obtain

$$\begin{aligned}
\mathbf{E}[\beta_0(\mathrm{Del}_r(Y;\Omega))] &= \frac{\sigma_{n-1}}{n\nu_n^{1-1/n}}\frac{1}{1-1/n}e^{-\rho\nu_n r^n}\rho\nu_n^{1-1/n}r^{n-1}\|\Omega\|\\
&= \frac{\sigma_{n-1}}{n-1}r^{n-1}e^{-\rho\nu_n r^n}\rho\|\Omega\| \qquad (24)\\
&= \nu_{n-1}r^{n-1}e^{-\rho\nu_n r^n}\rho\|\Omega\|, \qquad (25)
\end{aligned}$$

where we use the identity $\sigma_{n-1}/(n-1) = \nu_{n-1}$ in the last transition. In short, (25) gives an explicit formula for the expected density of connected components in the Boolean model in $\mathbf{R}^n$ intersected with a line. While the authors did not find the explicit expression in the literature, this result is not new and follows after some straightforward computations from [11, Excercise 4.8]. Our aim is to provide another, more topological view of the problem. The graphs of β_0 for different dimensions n are shown in Figure 5.

Using the Crofton formula [20, Theorem 9.4.7] (but see also [10]) and the fact that almost every connected component is a line segment that meets the boundary of the Boolean model in two points, (25) can be transformed into a statement about the boundary of X_r,

$$\overline{V}_{n-1}(X_r) = 2\sqrt{\pi}\,\frac{\Gamma(n/2)}{\Gamma((n+1)/2)}\nu_{n-1}r^{n-1}e^{-\rho\nu_n r^n}\rho, \qquad (26)$$

in which $\overline{V}_{n-1}(X_r)$ is the expected density of the $(n-1)$-dimensional volume of the boundary; see [20, section 9] for a detailed discussion of the quantity.

4. Anchored Blaschke–Petkantschin formula. To extend the results in the previous section from 1 to k dimensions, we first generalize the Blaschke–Petkantschin formula for spheres stated as Theorem 7.3.1 in [20].

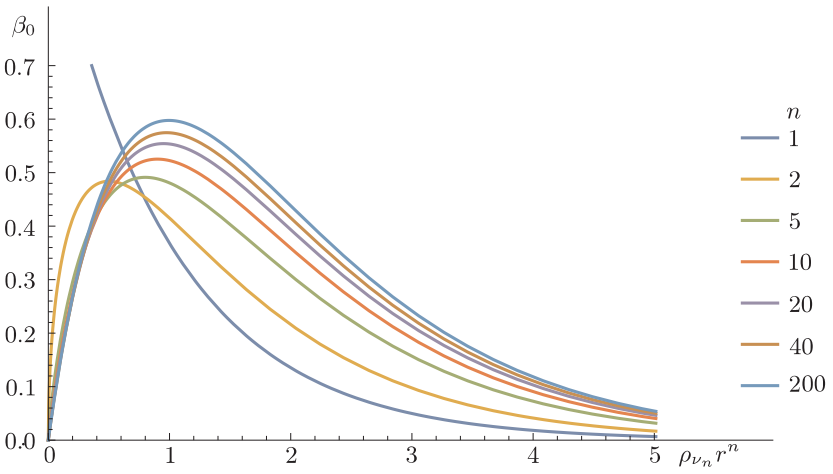

FIG. 5. *The expected number of connected components per unit length as a function of the radius. To facilitate the comparison of the graphs in different dimensions n, we rescale such that a unit along the horizontal axis is the expected number of points inside a ball of radius r in $\mathbf{R}^n$.*

Setting the stage. Recall that $k \leqslant n$ are positive integers, and that we write $\mathbf{R}^k$ for the k-dimensional linear subspace spanned by the first k coordinate vectors of $\mathbf{R}^n$. While we used uppercase letters to denote simplices in the previous sections, we now write $\mathbf{x}$ for a sequence of $m+1 \leqslant k+1$ points in $\mathbf{R}^n$. The reason for the change of notation is that we integrate over all such sequences and do not limit ourselves to points in the Poisson point process. Similarly, we write $\mathbf{u}$ if the $m+1$ points lie on the unit sphere. As usual, we do not distinguish between a simplex and its vertices, so we write $\mathrm{Vol}_m(\mathbf{x})$ for the m-dimensional Lebesgue measure of the convex hull of $\mathbf{x}$. Assuming that the $m+1$ points are in a general position in $\mathbf{R}^n$, the affine hull of $\mathbf{x}$ is an m-plane, $M = \operatorname{aff} \mathbf{x}$. Furthermore, the set of centers of the spheres that pass through all points of $\mathbf{x}$ is an $(n-m)$-plane, $M^\perp$, orthogonal to M. Generically, the intersection of $M^\perp$ with $\mathbf{R}^k$ is a plane of dimension $k-m$. The center of the smallest anchored sphere passing through $\mathbf{x}$ is the point of this intersection that is the closest to $\mathbf{x}$.

Top-dimensional case. We first show how to transform an integral over $m+1 = k+1$ points into the integral over a unique anchored sphere passing through these points.

LEMMA 1 (Blaschke–Petkantschin for top-dimensional simplices). *Let $0 \leqslant k \leqslant n$. Then every measurable nonnegative function $f\colon (\mathbf{R}^n)^{k+1} \to \mathbf{R}$ satisfies*

$$\begin{aligned} &\int_{\mathbf{x}\in(\mathbf{R}^n)^{k+1}} f(\mathbf{x})\,\mathrm{d}\mathbf{x} \\ &= \int_{y\in\mathbf{R}^k} \int_{r\geqslant 0} \int_{\mathbf{u}\in(\mathbb{S}^{n-1})^{k+1}} f(y+r\mathbf{u}) r^{(n-1)(k+1)} k!\,\mathrm{Vol}_k(\mathbf{u}')\,\mathrm{d}\mathbf{u}\,\mathrm{d}r\,\mathrm{d}y, \end{aligned} \tag{27}$$

in which $\mathbf{u}'$ is the projection of $\mathbf{u}$ to $\mathbf{R}^k$, $\mathrm{Vol}_k(\mathbf{u}')$ is the Lebesgue measure of the k-simplex, and we use the standard spherical measure on $\mathbb{S}^{n-1}$.

Proof. We follow the proof of Theorem 7.3.1 in [20], with just slight modifications. Recall first that we choose the coordinates in $\mathbf{R}^n$ so that the projection of

$x = (x_1, \dots, x_n)$ to $\mathbf{R}^k \hookrightarrow \mathbf{R}^n$ is $x' = (x_1, \dots, x_k, 0, \dots, 0)$. The claimed relation is a change of variables: on the right-hand side, we represent the points $\mathbf{x}$ by the center $y \in \mathbf{R}^k \hookrightarrow \mathbf{R}^n$ of the anchored sphere passing through these points, its radius r, and k points $\mathbf{u}$ on the unit sphere $\mathbb{S}^{n-1} \hookrightarrow \mathbf{R}^n$. This change of variables is the mapping $\varphi\colon \mathbf{R}^k \times [0,\infty) \times (\mathbb{S}^{n-1})^{k+1} \to (\mathbf{R}^n)^{k+1}$ defined by $\varphi(y, r, \mathbf{u}_0, \mathbf{u}_1, \dots, \mathbf{u}_k) = (y + r\mathbf{u}_0, y + r\mathbf{u}_1, \dots, y + r\mathbf{u}_k)$; we note that φ is bijective up to a measure 0 subset of the domain. We claim the Jacobian of φ is

$$J(y, r, \mathbf{u}) = r^{(n-1)(k+1)} k! \operatorname{Vol}_k(\mathbf{u}'), \tag{28}$$

in which $\mathbf{u}' = (\mathbf{u}'_0, \mathbf{u}'_1, \dots, \mathbf{u}'_k)$ is the projection of $\mathbf{u}$ to $\mathbf{R}^k$. To prove (28) at a particular point $(y, r, \mathbf{u})$, we choose local coordinates around every point $\mathbf{u}_i$ on the sphere. We choose them such that the matrix $[\mathbf{u}_i \dot{\mathbf{u}}_i]$ is orthogonal, for every $0 \leqslant i \leqslant k$, in which $\dot{\mathbf{u}}_i$ is the $(n \times (n-1))$-matrix of partial derivatives with respect to the $n-1$ local coordinates. This is the same parametrization as in [20]. With this, the Jacobian is the absolute value of the $(n(k+1) \times n(k+1))$-determinant

$$J(y, r, \mathbf{u}) = \operatorname{abs} \begin{vmatrix} E_{n,k} & \mathbf{u}_0 & r\dot{\mathbf{u}}_0 & 0 & \dots & 0 \\ E_{n,k} & \mathbf{u}_1 & 0 & r\dot{\mathbf{u}}_1 & \dots & 0 \\ \vdots & \vdots & \vdots & \vdots & \ddots & \vdots \\ E_{n,k} & \mathbf{u}_k & 0 & 0 & \dots & r\dot{\mathbf{u}}_k \end{vmatrix}, \tag{29}$$

where we write the matrix in block notation, with $E_{n,k}$ the $(n \times k)$-matrix with all elements zero and ones in the diagonal. Similarly, $\mathbf{u}_i$ is a column vector of length n, $r\dot{\mathbf{u}}_i$ is an $(n \times (n-1))$-matrix, and 0 is the zero matrix of appropriate size, which in this case is an $(n \times (n-1))$-matrix. As in [20], we extract r from $(k+1)(n-1)$ columns and use the fact that transposing the matrix does not affect the determinant to get

$$\left(\frac{J(y, r, \mathbf{u})}{r^{(k+1)(n-1)}}\right)^2 = \begin{vmatrix} E_{k,n} & E_{k,n} & \dots & E_{k,n} \\ \mathbf{u}_0^{\mathrm{T}} & \mathbf{u}_1^{\mathrm{T}} & \dots & \mathbf{u}_k^{\mathrm{T}} \\ \dot{\mathbf{u}}_0^{\mathrm{T}} & 0 & \dots & 0 \\ 0 & \dot{\mathbf{u}}_1^{\mathrm{T}} & \dots & 0 \\ \vdots & \vdots & \ddots & \vdots \\ 0 & 0 & \dots & \dot{\mathbf{u}}_k^{\mathrm{T}} \end{vmatrix} \cdot \begin{vmatrix} E_{n,k} & \mathbf{u}_0 & \dot{\mathbf{u}}_0 & 0 & \dots & 0 \\ E_{n,k} & \mathbf{u}_1 & 0 & \dot{\mathbf{u}}_1 & \dots & 0 \\ \vdots & \vdots & \vdots & \vdots & \ddots & \vdots \\ E_{n,k} & \mathbf{u}_k & 0 & 0 & \dots & \dot{\mathbf{u}}_k \end{vmatrix}. \tag{30}$$

The orthogonality of the matrices $[\mathbf{u}_i \dot{\mathbf{u}}_i]$ implies that $\mathbf{u}_i^{\mathrm{T}} \mathbf{u}_i = 1$, $\dot{\mathbf{u}}_i^{\mathrm{T}} \dot{\mathbf{u}}_i = E_{n-1,n-1}$, whereas $\mathbf{u}_i^{\mathrm{T}} \dot{\mathbf{u}}_i$ is the zero row vector of length $n-1$, and $\dot{\mathbf{u}}_i^{\mathrm{T}} \mathbf{u}_i$ is the zero column vector of length $n-1$, for each $0 \leqslant i \leqslant k$. We can therefore multiply the matrices and get

$$\left(\frac{J(y, r, \mathbf{u})}{r^{(k+1)(n-1)}}\right)^2 = \left|\begin{array}{cc:ccc} (k+1)E_{k,k} & \sum \mathbf{u}'_i & \dot{\mathbf{u}}'_0 & \dots & \dot{\mathbf{u}}'_k \\ \sum \mathbf{u}_i'^{\mathrm{T}} & k+1 & 0 & \dots & 0 \\ \hdashline \dot{\mathbf{u}}_0'^{\mathrm{T}} & 0 & E_{n-1,n-1} & \dots & 0 \\ \vdots & \vdots & \vdots & \ddots & \vdots \\ \dot{\mathbf{u}}_k'^{\mathrm{T}} & 0 & 0 & \dots & E_{n-1,n-1} \end{array}\right|, \tag{31}$$

in which we write $\mathbf{u}'_i$ for the vector consisting of the first k coordinates of $\mathbf{u}_i$. Similarly, $\dot{\mathbf{u}}'_i$ is the $(k \times (n-1))$-matrix obtained from $\dot{\mathbf{u}}_i$ by dropping the bottom $n-k$ rows.

As written, the $(n(k+1)\times n(k+1))$-matrix in (31) is a $((k+3)\times(k+3))$-matrix of blocks, all of which are not the same size. To zero out the last $k+1$ blocks in the first row, we subtract the third row times $\dot{\mathbf{u}}'_0$, the fourth row times $\dot{\mathbf{u}}'_1$, and so on. The determinant is therefore the product of the determinants of the upper left (2×2)-block matrix and the lower right $((k+1)\times(k+1))$-block matrix, the latter being 1. To further simplify the (2×2)-block matrix, we use $[\mathbf{u}_i\dot{\mathbf{u}}_i][\mathbf{u}_i\dot{\mathbf{u}}_i]^{\mathrm{T}} = E_{n,n}$, which implies $[\mathbf{u}'_i\dot{\mathbf{u}}'_i][\mathbf{u}'_i\dot{\mathbf{u}}'_i]^{\mathrm{T}} = E_{k,k}$, and we write the matrix as a product of two matrices,

$$\left(\frac{J(y,r,\mathbf{u})}{r^{(k+1)(n-1)}}\right)^2 = \begin{vmatrix} (k+1)E_{k,k} - \sum \dot{\mathbf{u}}'_i\dot{\mathbf{u}}_i'^{\mathrm{T}} & \sum \mathbf{u}'_i \\ \sum \mathbf{u}_i'^{\mathrm{T}} & k+1 \end{vmatrix} \tag{32}$$

$$= \begin{vmatrix} \sum \mathbf{u}'_i\mathbf{u}_i'^{\mathrm{T}} & \sum \mathbf{u}'_i \\ \sum \mathbf{u}_i'^{\mathrm{T}} & k+1 \end{vmatrix} = \left| \begin{bmatrix} \mathbf{u}'_0 & \mathbf{u}'_1 & \dots & \mathbf{u}'_k \\ 1 & 1 & \dots & 1 \end{bmatrix} \begin{bmatrix} \mathbf{u}_0'^{\mathrm{T}} & 1 \\ \mathbf{u}_1'^{\mathrm{T}} & 1 \\ \vdots & \vdots \\ \mathbf{u}_k'^{\mathrm{T}} & 1 \end{bmatrix} \right|, \tag{33}$$

in which we move from (32) to (33) using $\dot{\mathbf{u}}'_i\dot{\mathbf{u}}_i'^{\mathrm{T}} = E_{k,k} - \mathbf{u}'_i\mathbf{u}_i'^{\mathrm{T}}$. Finally, the determinant of the vectors $\mathbf{u}'_i$ with appended 1 is $k!$ times the k-dimensional volume of $\mathbf{u}'$. Hence, $J(y,r,\mathbf{u}) = r^{(k+1)(n-1)}k!\,\mathrm{Vol}_k(\mathbf{u}')$, as claimed in (28). This completes the proof of (27).

General case. Further, we generalize to the case $m \leqslant k$. Recall that for a sequence $\mathbf{x}$ of $m+1 \leqslant k+1$ points in $\mathbf{R}^n$, there is a unique smallest anchored sphere passing through them. We claim that its center lies inside the orthogonal projection P of the m-dimensional affine hull of $\mathbf{x}$ onto $\mathbf{R}^k$. Indeed, by orthogonally projecting the center of any anchored sphere passing through $\mathbf{x}$ to P in $\mathbf{R}^k$, we clearly get a point, which is a center of a smaller anchored sphere still passing through $\mathbf{x}$. The following theorem tells us how to integrate over these smallest anchored circumscribed spheres.

THEOREM 2 (anchored Blaschke–Petkantschin formula). *Let $0 \leqslant m \leqslant k \leqslant n$ and $\alpha = n(m+1)-(k+1)$. Then every measurable nonnegative function $f\colon (\mathbf{R}^n)^{m+1} \to \mathbf{R}$ satisfies*

$$\begin{aligned} &\int_{\mathbf{x}\in(\mathbf{R}^n)^{m+1}} f(\mathbf{x})\,\mathrm{d}\mathbf{x} \\ &= \int_{y\in\mathbf{R}^k}\int_{P\in\mathcal{L}^k_m}\int_{r\geqslant 0}\int_{\mathbf{u}\in(S)^{m+1}} f(y+r\mathbf{u})r^{\alpha}[m!\,\mathrm{Vol}_m(\mathbf{u}')]^{k-m+1}\,\mathrm{d}\mathbf{u}\,\mathrm{d}r\,\mathrm{d}P\,\mathrm{d}y, \end{aligned} \tag{34}$$

in which $\mathcal{L}^k_m$ is the Grassmannian of (linear) m-planes in $\mathbf{R}^k$, $\mathbf{u}'$ is the projection of $\mathbf{u}$ to P, and S is short for the unit sphere in $P\times\mathbf{R}^{n-k}$.

Proof. We use the Blaschke–Petkantschin formula twice, first in its standard form. For $P\in\mathcal{L}^k_m$, we write $P\times\mathbf{R}^{n-k}\in\mathcal{L}^n_{m+n-k}$ for the $(m+n-k)$-plane, whose orthogonal projection to $\mathbf{R}^k$ is P. The first application of the Blaschke–Petkantschin formula integrates over all (affine) m-planes in $\mathbf{R}^k$, spanned by the projections of $\mathbf{x}$ to $\mathbf{R}^k$:

$$\begin{aligned} &\int_{\mathbf{x}\in(\mathbf{R}^n)^{m+1}} f(\mathbf{x})\,\mathrm{d}\mathbf{x} \\ &= \int_{P\in\mathcal{L}^k_m}\int_{h\in P^{\perp}}\int_{\mathbf{x}\in(P\times\mathbf{R}^{n-k})^{m+1}} f(h+\mathbf{x})[m!\,\mathrm{Vol}_m(\mathbf{x}')]^{k-m}\,\mathrm{d}\mathbf{x}\,\mathrm{d}h\,\mathrm{d}P. \end{aligned} \tag{35}$$

For every m-plane P in $\mathbf{R}^k$, we consider the vertical $(m+n-k)$-plane $P \times \mathbf{R}^{n-k}$ in $\mathbf{R}^n$ and apply Lemma 1 inside it. Recalling that S is a unit sphere in $P \times \mathbf{R}^{n-k}$, this gives

$$\int_{\mathbf{x}\in(\mathbf{R}^n)^{m+1}} f(\mathbf{x})\,\mathrm{d}\mathbf{x}$$

$$= \int_{P\in\mathcal{L}^k_m}\int_{h\in P^\perp}\int_{z\in P}\int_{r\geqslant 0}\int_{\mathbf{u}\in(S)^{m+1}} f(h+z+r\mathbf{u})r^{(m+n-k-1)(m+1)} \tag{36}$$

$$\times\, m!\,\mathrm{Vol}_m(\mathbf{u}')[m!\,\mathrm{Vol}_m(r\mathbf{u}')]^{k-m}\,\mathrm{d}\mathbf{u}\,\mathrm{d}r\,\mathrm{d}z\,\mathrm{d}h\,\mathrm{d}P. \tag{37}$$

Note that $\mathrm{Vol}_m(r\mathbf{u}') = r^m\,\mathrm{Vol}_m(\mathbf{u}')$, which implies that the final power of r is $(m+n-k-1)(m+1)+m(k-m) = \alpha$. Finally, we get the claimed relation by setting $y = z+h$ and exchanging the integral over $P\in\mathcal{L}^k_m$ with the integral over $y\in\mathbf{R}^k$.

5. Expected number of intervals. In this section, we use the anchored Blaschke–Petkantschin formula of the previous section to compute the expected numbers of intervals of a weighted Delaunay mosaic in $\mathbf{R}^k$. We do this for every type and use a weighted Delaunay radius threshold to get more detailed probabilistic information. Recall that the weighted mosaic is a random k-dimensional slice of the (unweighted) Poisson–Delaunay mosaic with density $\rho>0$ in $\mathbf{R}^n$.

Slivnyak–Mecke formula. To count the type (ℓ,m) intervals, we focus our attention by restricting the center of the weighted Delaunay sphere to a region $\Omega\subseteq\mathbf{R}^k$ and the weighted Delaunay radius to be less than or equal to r_0. Any sequence $\mathbf{x}=(\mathbf{x}_0,\mathbf{x}_1,\dots,\mathbf{x}_m)$ of $m+1$ points in $\mathbf{R}^n$ defines such an interval if it satisfies the following conditions:

(a) The smallest anchored sphere passing through $\mathbf{x}$ is empty, and we write $\mathbf{P}_\varnothing(\mathbf{x})$ for the probability of this event;

(b) the center z of this sphere lies in Ω, and we write $\mathbf{1}_\Omega(\mathbf{x})$ for the indicator;

(c) the radius r of this sphere is bounded from above by r_0, and we write $\mathbf{1}_{r_0}(\mathbf{x})$ for the indicator;

(d) the origin of $\mathbf{R}^k$ sees exactly $m-\ell$ facets of the projected m-simplex from the outside, and we write $\mathbf{1}_{m-\ell}(\mathbf{x})$ for the indicator.

These are the same conditions as in [7] and [3] with the only difference being that the sphere is now required to be anchored, and modulo this remark the proofs are identical. Combining these conditions with the Slivnyak–Mecke formula, we get an integral expression for the expected number of type (ℓ,m) intervals, which we partially evaluate using Theorem 2 and Lemma 2:

$$\mathbf{E}[c^{k,n}_{\ell,m}(r_0)] = \frac{1}{(m+1)!}\int_{\mathbf{x}\in(\mathbf{R}^n)^{m+1}} \mathbf{P}_\varnothing(\mathbf{x})\mathbf{1}_\Omega(\mathbf{x})\mathbf{1}_{r_0}(\mathbf{x})\mathbf{1}_{m-\ell}(\mathbf{x})\,\mathrm{d}\mathbf{x} \tag{38}$$

$$= \|\Omega\|\|\mathcal{L}^k_m\|\rho^{m+1}\frac{m!^{k-m+1}}{(m+1)!}\int_{r\leqslant r_0} e^{-\rho\nu_n r^n} r^\alpha\,\mathrm{d}r$$

$$\times \int_{\mathbf{u}\in(S)^{m+1}} \mathbf{1}_{m-\ell}(\mathbf{u})\mathrm{Vol}_m(\mathbf{u}')^{k-m+1}\,\mathrm{d}\mathbf{u} \tag{39}$$

$$= \|\Omega\|\rho^{k/n}\frac{m!^{k-m}}{m+1}\|\mathcal{L}^k_m\|\frac{\gamma(m+1-k/n;\,\rho\nu_n r_0^n)}{n\nu_n^{m+1-k/n}}$$

$$\times \int_{\mathbf{u}\in(S)^{m+1}} \mathbf{1}_{m-\ell}(\mathbf{u})\mathrm{Vol}_m(\mathbf{u}')^{k-m+1}\,\mathrm{d}\mathbf{u} \tag{40}$$

$$= C^{k,n}_{\ell,m} \cdot \frac{\gamma(m+1-k/n;\, \rho\nu_n r_0^n)}{\Gamma(m+1-k/n)} \cdot \|\Omega\| \rho^{k/n}. \tag{41}$$

Specifically, we get (39) by noting $\mathbf{P}_\varnothing(\mathbf{x}) = e^{-\rho\nu_n r^n}$, applying Theorem 2 to the right-hand side of (38), collapsing the indicators, using rotational invariance, and writing S for the unit sphere in $\mathbf{R}^{m+n-k}$. We get (40) from (39) by applying Lemma 2 with $j = \alpha+1 = n(m+1)-k$, $c = \rho\nu_n$, $p = n$, $t_0 = r_0$, which asserts that the integral over the radius evaluates to the fraction involving the incomplete Gamma function. Finally, we get (41) by defining the constant

$$C^{k,n}_{\ell,m} = \frac{m!^{k-m} \|\mathcal{L}^k_m\| \Gamma(m+1-k/n)}{(m+1) n \nu_n^{m+1-k/n}} \int_{\mathbf{u}\in(S)^{m+1}} \mathbf{1}_{m-\ell}(\mathbf{u}) \mathrm{Vol}_m(\mathbf{u}')^{k-m+1} \,\mathrm{d}\mathbf{u}. \tag{42}$$

As a sanity check, we get $C^{1,n}_{0,0} = \sigma_{n-1}\Gamma(1-1/n)/(n\nu_n^{1-1/n})$ with $\ell = m = 0$ and $k = 1$, because $S \subseteq \mathbf{R}^{n-1}$ has volume σ_{n-1}, and we have $\mathbf{1}_0(\mathbf{u}_0) = 1$ and $\mathrm{Vol}_0(\mathbf{u}_0) = 1$ for all points $\mathbf{u}_0 \in S$. This agrees with (15) in section 2.

Simplices in the weighted Delaunay mosaic. Since the expression in (42) does not depend on r_0, we deduce that the weighted Delaunay radius of a typical type (ℓ, m) interval is Gamma-distributed. The weighted Delaunay radius of a typical j-simplex in the weighted Poisson–Delaunay mosaic therefore follows a linear combination of Gamma distributions. Indeed, we get the total number of j-simplices to be $d^{k,n}_j = \sum_{\ell=0}^{j} \sum_{m=j}^{k} \binom{m-\ell}{m-j} c^{k,n}_{\ell,m}$; see [7]. The same relation holds if we limit the simplices to a weighted Delaunay radius of at most r_0, and also if we replace the simplex counts by the constants $C^{k,n}_{\ell,m}$ and the analogously defined $D^{k,n}_j$. Before continuing, we consider the top-dimensional case, $j = k$, in which $D^{k,n}_k = \sum_{\ell=0}^{k} C^{k,n}_{\ell,k}$. Taking the sum eliminates the indicator function in (42), and we get

$$D^{k,n}_k = \frac{\Gamma(k+1-k/n)}{(k+1) n \nu_n^{k+1-k/n}} \int_{\mathbf{u}\in(\mathbb{S}^{n-1})^{k+1}} \mathrm{Vol}_k(\mathbf{u}') \,\mathrm{d}\mathbf{u}. \tag{43}$$

We can compare this with the expression for the number of Voronoi vertices by Møller [16] using the Crofton formula [10, Chap. 6]; see also [20, Theorem 10.2.4]. By duality, the number of vertices in the weighted Voronoi tessellation is the number of top-dimensional simplices in the weighted Delaunay mosaic. Each vertex is the intersection of an $(n-k)$-dimensional Voronoi polyhedron with the k-plane, and if we know the expected number of intersections, then we also know the integral over all k-planes. The Crofton formula applies and gives the $(n-k)$-dimensional volume of the $(n-k)$-skeleton of the Voronoi tessellation as $\sigma_n/(2\|\mathcal{L}^n_k\|\nu_{n-1})$ times the mentioned integral. It turns out that the expected volume is not so difficult to compute otherwise [16], so we can turn the argument around and deduce the expected number of vertices from the expected $(n-k)$-dimensional volume. This gives

$$\begin{aligned} D^{k,n}_k = {} & \frac{\sigma_1\sigma_{n+1}}{\sigma_{k+1}\sigma_{n-k+1}} \frac{2^{k+1}\pi^{k/2}}{n(k+1)!} \frac{\Gamma((kn+n-k+1)/2)}{\Gamma((kn+n-k)/2)} \\ & \times \frac{\Gamma((n+2)/2)^{k+1-k/n}}{\Gamma((n+1)/2)^k} \frac{\Gamma(k+1-k/n)}{\Gamma(n-k+1/2)}. \end{aligned} \tag{44}$$

Comparing (44) with (43), we get an explicit expression for the expected k-dimensional volume of the projection of a random k-simplex inscribed in $\mathbb{S}^{n-1}$.

6. Computations. We now return to (42) and note that the integral on the right-hand side is σ_{m+n-k}^{m+1} times the expected value of the random variable (r.v.)

$$U_{\ell,m}^{k,n} = \mathbf{1}_{m-\ell}(\mathbf{u}) \operatorname{Vol}_m(\mathbf{u}')^{k-m+1}, \tag{45}$$

where $\mathbf{u}$ is a sequence of $m+1$ random points uniformly and independently distributed on the unit sphere in $\mathbf{R}^{m+n-k}$, and $\mathbf{u}'$ is the corresponding sequence of points projected to $\mathbf{R}^m \hookrightarrow \mathbf{R}^{m+n-k}$. Our goal is to compute $\mathbf{E}[U_{\ell,m}^{k,n}]$ in some special cases. Instead of working with the original points, we prefer to study their projections to $\mathbf{R}^m$, but the distribution of the $m+1$ points in $\mathbf{R}^m$ has yet to be determined. If the upper bound is a vertex or an edge, then we find explicit expressions of the expected number of intervals.

Critical vertices. For $m = 0$, we count the intervals of type $(0, 0)$ or, equivalently, the critical vertices. Since $U_{0,0}^{k,n} = 1$, for all $k \leqslant n$, we get

$$C_{0,0}^{k,n} = \sigma_{n-k} \frac{\Gamma(1 - k/n)}{n\nu_n^{1-k/n}} \tag{46}$$

from (42). Accordingly, the expected number of critical vertices in Ω with weighted Delaunay radius at most r_0 is $C_{0,0}^{k,n}$ times the normalized incomplete Gamma function times $\|\Omega\|\rho^{k/n}$; compare with (5) and (6) in section 2.

Vertex-edge pairs. Further, we count the intervals of type $(0, 1)$ or, equivalently, the regular vertex-edge pairs. For this, we need the expectation of $U_{0,1}^{k,n}$: picking two random points on the unit sphere in $\mathbf{R}^{n-k+1}$ and projecting them to $\mathbf{R}^1 \hookrightarrow \mathbf{R}^{n-k+1}$, this is the expectation when we get the kth power of the distance between the projected points if they lie on the same side of the origin, and we get 0 otherwise. Writing $\mathbf{u}_0', \mathbf{u}_1' \in [-1, 1]$ for the projected points and $x = |\mathbf{u}_0'|$, $y = |\mathbf{u}_1'|$ for their absolute values, we note that the signs and magnitudes are independent. It follows that we get zero with probability $1/2$, so the desired expectation is

$$\mathbf{E}[U_{0,1}^{k,n}] = \frac{1}{2}\mathbf{E}[|x - y|^k] = \mathbf{E}[(x - y)^k \mathbf{1}_{x>y}]. \tag{47}$$

We can therefore restrict our attention to the half of the unit sphere that projects onto $[0, 1]$. To integrate over this hemisphere, we use the fact that x^2 and y^2 are independent Beta-distributed r.v.'s; see Appendix A. Setting $a = x^2$ and $b = y^2$, we have

$$\begin{aligned}
\mathbf{E}[U_{0,1}^{k,n}] &= \frac{1}{B((n-k)/2, 1/2)^2} \\
&\quad \times \int_{a=0}^{1} \int_{b=0}^{a} [\sqrt{a} - \sqrt{b}]^k a^{-1/2}(1-a)^{(n-k-2)/2} b^{-1/2}(1-b)^{(n-k-2)/2} \,\mathrm{d}a\,\mathrm{d}b \qquad (48) \\
&= \frac{4}{B((n-k)/2, 1/2)^2} \\
&\quad \times \int_{x=0}^{1} \int_{y=0}^{x} [x - y]^k (1-x^2)^{(n-k-2)/2} (1-y^2)^{(n-k-2)/2} \,\mathrm{d}x\,\mathrm{d}y \qquad (49) \\
&= \frac{\Gamma(k+1)\Gamma((n-k+1)/2)^2}{2^k\sqrt{\pi}\,\Gamma((n-k)/2)^2} \cdot {}_3\widetilde{F}_2\left(\frac{1}{2}, 1, \frac{k-n+2}{2}; \frac{k+3}{2}, \frac{n+2}{2}; 1\right), \qquad (50)
\end{aligned}$$

in which ${}_3\widetilde{F}_2$ is the regularized hypergeometric function considered in Appendix A, and we use Mathematica to move from (49) to (50). As mentioned at the end of Appendix A,

$$\frac{k+3}{2} + \frac{n+2}{2} > \frac{1}{2} + 1 + \frac{k-n+2}{2}$$

is a sufficient condition for the convergence of the infinite sum that defines the value of the regularized hypergeometric function. This is equivalent to the inequality $n > 0$, which is always satisfied. Plugging (50) into (42), we get the following expression for the corresponding constant:

$$\begin{aligned} C^{k,n}_{0,1} &= \frac{\sigma^2_{n-k+1}\sigma_k\Gamma(2-k/n)}{4n\nu_n^{2-k/n}} \, \frac{\Gamma(k+1)\Gamma((n-k+1)/2)^2}{2^k\sqrt{\pi}\,\Gamma((n-k)/2)} \\ &\quad \times {}_3\widetilde{F}_2\bigg(\frac{1}{2}, 1, \frac{k-n+2}{2}; \frac{k+3}{2}, \frac{n+2}{2}; 1\bigg). \end{aligned} \tag{51}$$

Critical edges. Further, we count the intervals of type $(1, 1)$ or, equivalently, the critical edges. Here the expectation of $U^{k,n}_{1,1}$ is relevant: picking two points on the unit sphere in $\mathbf{R}^{n-k+1}$ and projecting them onto $\mathbf{R}^1 \hookrightarrow \mathbf{R}^{n-k+1}$, this is the expectation in which we get the kth power of the distance between the projected points if they lie on opposite sides of the origin, and we get 0 otherwise. Using again the fact that the signs and magnitude of the projected points are independent, we note that this expectation is $\mathbf{E}[U^{k,n}_{1,1}] = (1/2)\mathbf{E}[(x+y)^k]$. Setting $a = x^2$, $b = y^2$ and integrating as before, we get

$$\begin{aligned} \mathbf{E}[U^{k,n}_{1,1}] &= \frac{1}{B((n-k)/2, 1/2)^2} \\ &\quad \times \int_{a=0}^1 \int_{b=0}^1 [\sqrt{a} + \sqrt{b}]^k a^{-1/2}(1-a)^{(n-k-2)/2} b^{-1/2}(1-b)^{(n-k-2)/2} \,\mathrm{d}a\,\mathrm{d}b \qquad (52) \\ &= \frac{1}{B((n-k)/2, 1/2)^2} \\ &\quad \times \int_{a=0}^1 \int_{b=0}^1 \sum_{i=0}^k \binom{k}{i} a^{(i-1)/2} b^{(k-i-1)/2} (1-a)^{(n-k-2)/2} (1-b)^{(n-k-2)/2} \,\mathrm{d}a\,\mathrm{d}b \qquad (53) \\ &= \frac{1}{B((n-k)/2, 1/2)^2} \sum_{i=0}^k \binom{k}{i} B\bigg(\frac{n-k}{2}, \frac{i+1}{2}\bigg) B\bigg(\frac{n-k}{2}, \frac{k-i+1}{2}\bigg). \qquad (54) \end{aligned}$$

Plugging (54) into (42), we get the following expression for the corresponding constant:

$$\begin{aligned} C^{k,n}_{1,1} &= \frac{\sigma^2_{n-k+1}\sigma_k\Gamma(2-k/n)}{8n\nu_n^{2-k/n} B((n-k)/2, 1/2)^2} \\ &\quad \times \sum_{i=0}^k \binom{k}{i} B\bigg(\frac{n-k}{2}, \frac{i+1}{2}\bigg) B\bigg(\frac{n-k}{2}, \frac{k-i+1}{2}\bigg). \end{aligned} \tag{55}$$

Constants in low dimensions. The authors have checked the k-dimensional formulas against the 1-dimensional formulas in section 2, both symbolically and numerically. In $k = 2$ dimensions, the formulas provide sufficient information to compute all constants governing the expectations of the six types of intervals. We get three

constants from (46), (51), (55):

$$C_{0,0}^{2,n} = \frac{\sigma_{n-2}\Gamma(1-2/n)}{n\nu_n^{1-2/n}}, \tag{56}$$

$$C_{0,1}^{2,n} = \frac{\sigma_{n-1}^2\sqrt{\pi}\,\Gamma(2-2/n)}{4n\nu_n^{2-2/n}}\,\frac{\Gamma((n-1)/2)^2}{\Gamma((n-2)/2)}\cdot {}_3\widetilde{F}_2\left(\frac{1}{2},1,\frac{4-n}{2};\,\frac{5}{2},\frac{n+2}{2};\,1\right), \tag{57}$$

$$C_{1,1}^{2,n} = \frac{\sigma_{n-1}^2\Gamma(2-2/n)\pi}{2n\nu_n^{2-2/n}}\cdot\left[\frac{1}{n-1}+\frac{\Gamma((n-1)/2)^2}{\pi\Gamma(n/2)^2}\right]. \tag{58}$$

The critical simplices satisfy the Euler relation [8]: $C_{0,0}^{2,n} - C_{1,1}^{2,n} + C_{2,2}^{2,n} = 0$, which gives us the constant for the critical triangles. We get another linear relation from the fact that in the plane the number of triangles is twice the number of vertices [20, Thm. 10.1.2, p. 458]: $C_{0,2}^{2,n} + C_{1,2}^{2,n} + C_{2,2}^{2,n} = 2(C_{0,0}^{2,n} + C_{0,1}^{2,n} + C_{0,2}^{2,n})$. Finally, we get a relation for the number of weighted Delaunay triangles from (44), which we restate for $k = 2$:

$$D_2^{2,n} = \frac{2\sigma_{n+1}}{3n\sigma_{n-1}}\,\frac{\Gamma((3n-1)/2)}{\Gamma((3n-2)/2)}\,\frac{\Gamma((n+2)/2)^{3-2/n}}{\Gamma((n+1)/2)^2}\,\frac{\Gamma(3-2/n)}{\Gamma((n-1)/2)}. \tag{59}$$

Combining $C_{0,2}^{2,n} + C_{1,2}^{2,n} + C_{2,2}^{2,n} = D_2^{2,n}$ with the two linear relations mentioned above, we get

$$C_{0,2}^{2,n} = -C_{0,0}^{2,n} - C_{0,1}^{2,n} + \frac{1}{2}D_2^{2,n}, \tag{60}$$

$$C_{1,2}^{2,n} = C_{0,0}^{2,n} + C_{0,1}^{2,n} - C_{2,2}^{2,n} + \frac{1}{2}D_2^{2,n}, \tag{61}$$

$$C_{2,2}^{2,n} = -C_{0,0}^{2,n} + C_{1,1}^{2,n}. \tag{62}$$

For small values of n, the constants are approximated in Table 2.

TABLE 2

The rounded constants in the expressions of the expected number of intervals and simplices of a 2-dimensional weighted Delaunay mosaic obtained from a Poisson point process in n dimensions.

	$n=3$	4	5	6	7	8	9	10	...	20	...	1000
$C_{0,0}^{2,n}$	1.11	1.25	1.38	1.49	1.58	1.66	1.73	1.79	...	2.12	...	2.69
$C_{0,1}^{2,n}$	0.26	0.42	0.54	0.63	0.71	0.77	0.82	0.86	...	1.12	...	1.54
$C_{0,2}^{2,n}$	0.09	0.15	0.21	0.25	0.28	0.31	0.33	0.35	...	0.47	...	0.65
$C_{1,1}^{2,n}$	2.47	2.92	3.30	3.61	3.87	4.09	4.28	4.44	...	5.37	...	6.92
$C_{1,2}^{2,n}$	1.46	1.83	2.13	2.37	2.57	2.74	2.89	3.01	...	3.72	...	4.88
$C_{2,2}^{2,n}$	1.37	1.67	1.92	2.12	2.29	2.43	2.55	2.66	...	3.25	...	4.23
$D_0^{2,n}$	1.46	1.83	2.13	2.37	2.57	2.74	2.89	3.01	...	3.72	...	4.88
$D_1^{2,n}$	4.37	5.48	6.38	7.10	7.71	8.22	8.66	9.03	...	11.16	...	14.65
$D_2^{2,n}$	2.92	3.66	4.25	4.74	5.14	5.48	5.77	6.02	...	7.44	...	9.77

7. Discussion. The main result of this paper is the stochastic analysis of the radius function of a weighted Poisson–Delaunay mosaic. As a consequence, we get formulas for the expected number of simplices in weighted Poisson–Delaunay mosaics (cf. [12], [13]). The main technical steps leading up to this result are a new

Blaschke–Petkantschin formula for spheres, stated as Theorem 2, and the discrete Morse theory approach recently introduced in [7].

There are a number of open questions that remain:

(1) We have explicit expressions for the constants in the expected number of intervals of all types for dimension $k \leqslant 2$. To go beyond two dimensions, Wendel's method of reflecting vertices of a simplex through the origin [23] should be useful. Short of getting precise formulas, can we say something about the asymptotic behavior of the constants, as k and n go to infinity?

(2) The connection to the Crofton formula and the volumes of Voronoi skeleta has been mentioned in section 5. Are there further connections that relate such volumes with simplices of dimension strictly less than k, or with subsets of simplices limited to radii at most r_0?

(3) The slice construction implies a repulsive force among the vertices: the vertices of the weighted Poisson–Delaunay mosaic are more evenly spread than a Poisson point process. For fixed k, the repulsion gets stronger with increasing n. It would be interesting to analytically study this repulsive force and its consequences.

Appendix A. On special functions. In this appendix, we define and discuss three types of special functions used in the main part of this paper: Gamma functions, Beta functions, and hypergeometric functions.

Gamma functions. We recall that the *lower-incomplete Gamma function* takes two parameters, j and $t_0 \geqslant 0$, and is defined by

$$\gamma(j;t_0) = \int_{t=0}^{t_0} t^{j-1}e^{-t}\,\mathrm{d}t. \tag{63}$$

The corresponding complete *Gamma function* is $\Gamma(j) = \gamma(j;\infty)$. An important relation for Gamma functions is $\Gamma(j+1) = j\,\Gamma(j)$, which holds for any real j that is not a nonpositive integer. We often use the ratio, $\gamma(j;t_0)/\Gamma(j)$, which is the density of a probability distribution and called the *Gamma distribution* with parameter j. We prove a technical lemma about incomplete Gamma functions, which is repeatedly used in the main part of this paper.

Lemma 2 (Gamma function). *Let $c, p, j, t_0 \in \mathbf{R}$ with $p \neq 0$ and $t_0 > 0$. Then*

$$\int_{t=0}^{t_0} t^{j-1}e^{-ct^p}\,\mathrm{d}t = \frac{\gamma(j/p;\, ct_0^p)}{pc^{j/p}}. \tag{64}$$

Proof. We rewrite the numerator on the right-hand side of (64) using the definition of the right-incomplete Gamma function (63) and substituting $u = ct^p$ and $\mathrm{d}u = cpt^{p-1}\,\mathrm{d}t$:

$$\gamma\left(\frac{j}{p};\, ct_0^p\right) = \int_{u=0}^{ct_0^p} u^{j/p-1}e^{-u}\,\mathrm{d}u \tag{65}$$

$$= \int_{t=0}^{t_0} (ct^p)^{j/p-1}e^{-ct^p}\,cpt^{p-1}\,\mathrm{d}t \tag{66}$$

$$= \int_{t=0}^{t_0} pc^{j/p}t^{j-1}e^{-ct^p}\,\mathrm{d}t. \tag{67}$$

Dividing by $pc^{j/p}$ gives the claimed relation.

Beta functions. Given real numbers a, b, and $0 \leqslant t_0 \leqslant 1$, the *incomplete Beta function* is defined by

$$B_{t_0}(a,b) = \int_{t=0}^{t_0} t^{a-1}(1-t)^{b-1}\,\mathrm{d}t, \tag{68}$$

and the complete *Beta function* is $B(a,b) = B_1(a,b)$, which can be expressed in terms of complete Gamma functions as $B(a,b) = \Gamma(a)\Gamma(b)/\Gamma(a+b)$.

The Beta functions can be used to integrate over the projection of a sphere in $\mathbf{R}^n$ to a linear subspace $\mathbf{R}^k \hookrightarrow \mathbf{R}^n$, as we now explain. Assuming that $\mathbf{R}^k$ is spanned by the first k coordinate vectors of $\mathbf{R}^n$, the projection of a point means dropping coordinates from $k+1$ to n. Suppose now that we pick a point $x = (x_1, \ldots, x_n)$ uniformly on $\mathbb{S}^{n-1}$ by normalizing a vector of n normally distributed r.v.'s: $X_i \sim \mathcal{N}(0,1)$, $1 \leqslant i \leqslant n$, and $x_j = X_j / \left(\sum_{i=1}^n X_i^2\right)^{1/2}$ for $1 \leqslant j \leqslant n$. Its projection to $\mathbf{R}^k$ is $x' = (x_1, \ldots, x_k, 0, \ldots, 0)$, and the squared distance from the origin is $\|x'\|^2 = \left(\sum_{i=1}^k x_i^2\right)/\left(\sum_{i=1}^n x_i^2\right)$. This can be written as $r^2 = X/(X+Y)$, in which X and Y are χ^2-distributed independent r.v.'s with k and $n-k$ degrees of freedom, respectively. This implies that $r^2 \sim B(k/n, (n-k)/n)$ [22, section 4.2]. Consider, for example, the case $k = n-1$. Integrating in $\mathbf{R}^k$ over all points with distance at most r_0 from the origin is the same as integrating over two spherical caps of $\mathbb{S}^{n-1}$, namely the cap around the north pole bounded by $(n-2)$-spheres of radius r_0, and a similar cap around the south pole. To compute the volume of a single such cap, we set $t_0 = r_0^2$ and integrate the incomplete Beta function:

$$\begin{aligned} \mathrm{Vol}_{n-1}(r_0) &= \frac{\sigma_n}{2B((n-1)/2, 1/2)} \int_{t=0}^{t_0} t^{(n-1)/2-1}(1-t)^{1/2-1}\,\mathrm{d}t \\ &= \frac{B_{t_0}((n-1)/2)1/2}{2B((n-1)/2, 1/2)}. \end{aligned} \tag{69}$$

Similarly, we can integrate over a ball in a k-dimensional projection and get the volume of the preimage, which is a solid torus inside the $(n-1)$-sphere.

Hypergeometric functions. The family of *hypergeometric functions* takes $p+q$ parameters and one argument and can be defined as a sum of products of Gamma functions, while the *regularized* version of this function is obtained by normalizing by the product of $\Gamma(b_i)$:

$${}_pF_q(a_1, \ldots, a_p;\, b_1, \ldots, b_q;\, z) = \sum_{j=0}^{\infty} \left[\prod_{i=1}^{p} \frac{\Gamma(j+a_i)}{\Gamma(a_i)}\right] \left[\prod_{i=1}^{q} \frac{\Gamma(b_i)}{\Gamma(j+b_i)}\right] \frac{z^j}{j!}, \tag{70}$$

$${}_p\widetilde{F}_q(a_1, \ldots, a_p;\, b_1, \ldots, b_q;\, z) = {}_pF_q(a_1, \ldots, a_p;\, b_1, \ldots, b_q;\, z) \Big/ \prod_{i=1}^{q} \Gamma(b_i) \tag{71}$$

$$= \sum_{j=0}^{\infty} \left[\prod_{i=1}^{p} \frac{\Gamma(j+a_i)}{\Gamma(a_i)}\right] \left[\prod_{i=1}^{q} \frac{1}{\Gamma(j+b_i)}\right] \frac{z^j}{j!}. \tag{72}$$

We are interested in the type $p=3$ and $q=2$. Here convergence of the infinite sum depends on the values of the parameters. We always have convergence for $|z| < 1$, and if $z = 1$, a sufficient condition for convergence is $b_1 + b_2 > a_1 + a_2 + a_3$ (see [18]).

REFERENCES

[1] F. Aurenhammer, *Power diagrams: Properties, algorithms, and applications*, SIAM J. Comput., 16 (1987), pp. 78–96.

[2] F. Aurenhammer and H. Imai, *Geometric relations among Voronoi diagrams*, Geom. Dedicata, 27 (1988), pp. 65–75.

[3] U. Bauer and H. Edelsbrunner, *The Morse theory of Čech and Delaunay complexes*, Trans. Amer. Math. Soc., 369 (2017), pp. 3741–3762.

[4] L. Burtseva, F. Werner, B. Valdez, A. Pestriakov, R. Romero, and V. Petranovskii, *Tessellation methods for modeling the material structure*, Appl. Mech. Mater., 756 (2015), pp. 426–435.

[5] H. Edelsbrunner, *Geometry and Topology for Mesh Generation*, Cambridge Monogr. Appl. Comput. Math. 7, Cambridge Univ. Press, Cambridge, 2001.

[6] H. Edelsbrunner and J. L. Harer, *Computational Topology. An Introduction*, Amer. Math. Soc., Providence, RI, 2010.

[7] H. Edelsbrunner, A. Nikitenko, and M. Reitzner, *Expected sizes of Poisson–Delaunay mosaics and their discrete Morse functions*, Adv. in Appl. Probab., 49 (2017), pp. 745–767.

[8] R. Forman, *Morse theory for cell complexes*, Adv. Math., 134 (1998), pp. 90–145.

[9] I. M. Gelfand, M. M. Kapranov, and A. V. Zelevinsky, *Discriminants, Resultants, and Multidimensional Determinants*, Math. Theory Appl., Birkhäuser, Boston, MA, 1994.

[10] H. Hadwiger, *Vorlesungen über Inhalt, Oberfläche und Isoperimetrie*, Grundlehren Math. Wiss. 93, Springer-Verlag, Berlin, 1957.

[11] P. Hall, *Introduction to the Theory of Coverage Processes*, Wiley Ser. Probab. Math. Statist. Probab. Math. Statist., John Wiley & Sons, New York, 1988.

[12] C. Lautensack, *Random Laguerre Tessellations*, Ph.D. thesis, Department of Mathematics, University of Karlsruhe, Karlsruhe, 2007.

[13] C. Lautensack and S. Zuyev, *Random Laguerre tessellations*, Adv. in Appl. Probab., 40 (2008), pp. 630–650.

[14] R. E. Miles, *On the homogeneous planar Poisson point process*, Math. Biosci., 6 (1970), pp. 85–127.

[15] R. E. Miles, *Isotropic random simplices*, Adv. in Appl. Probab., 3 (1971), pp. 353–382.

[16] J. Møller, *Random tessellations in* $\mathbb{R}^d$, Adv. in Appl. Probab., 21 (1989), pp. 37–73.

[17] A. Okabe, B. Boots, K. Sugihara, and S. N. Chui, *Spatial Tessellations: Concepts and Applications of Voronoi Diagrams*, 2nd ed., Wiley Ser. Probab. Stat., John Wiley & Sons, Chichester, 2000.

[18] F. W. J. Olver, D. W. Lozier, R. F. Boisvert, and C. W. Clark, eds., *NIST Handbook of Mathematical Functions*, U.S. Department of Commerce, National Institute of Standards and Technology, Washington, DC, 2010.

[19] N. Prunet and E. M. Meyerowitz, *Genetics and plant development*, C. R. Biologies, 339 (2016), pp. 240–246.

[20] R. Schneider and W. Weil, *Stochastic and Integral Geometry*, Probab. Appl. (N.Y.), Springer-Verlag, Berlin, 2008.

[21] R. Sibson, *A vector identity for the Dirichlet tessellation*, Math. Proc. Cambridge Philos. Soc., 87 (1980), pp. 151–155.

[22] C. Walck, *Hand-book on Statistical Distributions for Experimentalists*, Internal Report SUF-PFY/96-01, Stockholm University, Stockholm, 1996.

[23] J. G. Wendel, *A problem in geometric probability*, Math. Scand., 11 (1962), pp. 109–111.